PRAMANA
— journal of
physics

Vol. 45, No. 2,
August 1995
pp. 149–164

Time dependent canonical perturbation theory II: Application to the Henon–Heiles system

MITAXI P MEHTA and B R SITARAM
Physical Research Laboratory, Navrangpura, Ahmedabad 380 009, India

MS received 10 May 1995

Abstract. In this communication, we report the results of the application of time-dependent perturbation theory to the Henon–Heiles system. We show that the predictions of the perturbation theory hold good for short times, and try to explain the increase of error in the predicted results with the increase in energy.

Keywords. Canonical perturbation; Henon–Heiles

PACS Nos 05·45; 03·20

1. Introduction

One of the fundamental problems in canonical perturbation theory is, given a Hamiltonian

$$H = H_0 + \varepsilon H_1, \tag{1}$$

where ε is a parameter, to determine a canonical transformation which transforms H_0 to H, as a power series in ε. In a previous paper [1], this was attempted by allowing the canonical transformation to be time-dependent and it was shown that the approach removes some of the singularities of canonical perturbation theory. The method introduced a new degree of freedom, by using time as a canonical coordinate, with T as its conjugate variable, and replacing the original Hamiltonian H by $H + T$. The salient features of the results were:

1. The generators of the canonical transformation were finite at every order of perturbation theory.
2. The generators at nth order of perturbation theory were $O(\varepsilon^n)$.

In this communication, we study the application of the theory to the Henon–Heiles Hamiltonian. In general, perturbation theory can be tested via two approaches, namely, the predictions regarding invariants and the solutions of the equations of motion (EOM). Both these tests have been performed using third order perturbation theory for the system under study.

The plan of the paper is as follows: In § 2, we review the Henon–Heiles system. Section 3 contains the basic formulae for the generators of the canonical transformation, the invariants and the solutions. In § 4 we present the numerical results. Section 5 concludes with a discussion on the convergence properties of the perturbation series.

2. The Henon–Heiles Hamiltonian

The Henon–Heiles system, which is known to be a chaotic system, was first studied by

Henon and Heiles [2] to investigate the integrability of motion in an axisymmetric potential. The Hamiltonian is a truncation of the Toda-lattice Hamiltonian [3] up to third-order terms and it is a model for motion of a star in an axisymmetric gravitational field. The Hamiltonian is given by,

$$H = \frac{p_1^2 + p_2^2 + q_1^2 + q_2^2}{2} + \varepsilon\left(q_1^2 q_2 - \frac{q_2^3}{3}\right), \tag{2}$$

where ε is the perturbation parameter. ε can be rescaled using the transformation,

$$q_i \rightarrow \frac{Q_i}{\varepsilon}$$

$$p_i \rightarrow \frac{P_i}{\varepsilon}$$

$i = 1, 2$ under which,

$$H \rightarrow \frac{1}{\varepsilon^2} h$$

where,

$$h = \frac{Q_1^2 + Q_2^2 + P_1^2 + P_2^2}{2} + Q_1^2 Q_2 - \frac{Q_2^3}{3}.$$

Thus solving for motion of Henon–Heiles system for one value of ε and different values of energy is equivalent to solving for one value of energy and different values of ε. Our approach here has been the first one i.e. we have fixed the value of ε to 0·01 and studied the system for different values of energy. (For comparison with other results, energies are always quoted for the equivalent Hamiltonian, h.)

Further the system shows a transition from regular behaviour to chaotic behaviour with the change in energy [2]. The following characteristics are well-known: for $E < 1/12$ the Poincare sections indicate regular motion, i.e., the section is filled with closed curves and there is no exponential divergence of trajectories. In the range $1/12 < E < 1/6$ the motion shows a transition from regular to chaotic behaviour, becoming more and more chaotic with increase in E, i.e, the area which is covered by closed curves in the section becomes smaller with increase in E. Beyond $E = 1/6$, the motion becomes non-compact, with solutions escaping to infinity. (There are unbounded orbits for all energies, including for those with $E < 1/6$; these orbits do not play any role in our analysis, as a suitable choice of initial conditions ensures that the orbits remain bounded.)

Classical perturbation theory is known to be singular for this Hamiltonian because of resonances [3], which arise at second order in perturbation theory. The KAM theorem [4] cannot be applied directly to the system; the condition,

$$\det\left(\frac{\partial \omega_i}{\partial I_j}\right) \neq 0$$

is not satisfied, as the unperturbed frequencies are independent of the actions. Gustavson's method [5] give good results for small energies but does not predict the chaotic behaviour of Poincare sections.

3. Generating functions, solutions and invariants

We take the unperturbed Hamiltonian as the two-dimensional harmonic oscillator Hamiltonian,

$$H_0' = \frac{p_1^2 + p_2^2 + q_1^2 + q_2^2}{2} + T \tag{3}$$

with

$$H_0 = \frac{p_1^2 + p_2^2 + q_1^2 + q_2^2}{2}$$

and the full Hamiltonian as,

$$H' = H_0 + \varepsilon H_1 + T \tag{4}$$

where,

$$H_1 = q_1^2 q_2 - \frac{q_2^3}{3} \tag{5}$$

where (t, T) are extra phase space coordinates [1], and the new Poisson bracket is defined as

$$\{f,g\}' = \frac{\partial f}{\partial t}\frac{\partial g}{\partial T} - \frac{\partial f}{\partial T}\frac{\partial g}{\partial t} + \{f,g\},$$

with $\{f,g\}$ denoting the usual Poisson bracket.

In unperturbed action-angle coordinates we get,

$$H_0' = I_1 + I_2 + T, \tag{6}$$

$$H_1 = 2I_1 \cos^2\theta_1 \sqrt{2I_2}\cos\theta_2 - \frac{(\sqrt{2I_2}\cos\theta_2)^3}{3}. \tag{7}$$

The equations determining the generators are,

$$\{F_1, H_0'\}' = H_1 \tag{8}$$

$$\{F_2, H_0'\}' = -\frac{\{F_1,\{F_1, H_0'\}'\}'}{2} \tag{9}$$

$$\{F_3, H_0'\}' = -\frac{\{F_1,\{F_1,\{F_1, H_0'\}'\}'\}'}{3!} - \{F_2,\{F_1, H_0'\}'\}' \tag{10}$$

The F's were calculated using Mathematica programs. The expressions for the generating functions are given in the appendix.

Accordingly the constants of motion for H to third order are given by,

$$I_i' = I_i + \varepsilon\{F_1, I_i\}' + \frac{\varepsilon^2\{F_1,\{F_1, I_i\}'\}'}{2} + \frac{\varepsilon^3\{F_1,\{F_1,\{F_1, I_i\}'\}'\}'}{3!}$$
$$+ \varepsilon^2\{F_2, I_i\}' + \varepsilon^3\{F_2,\{F_1, I_i\}'\}' + \varepsilon^3\{F_3, I_i\}' \tag{11}$$

where $i = 1, 2$.

The solutions of the EOM for H can be obtained from those of H_0 using the equations

$$\xi_i = \xi_i' - \varepsilon\{F_1, \xi_i'\}' + \varepsilon^2 \frac{\{F_1, \{F_1, \xi_i'\}'\}'}{2} - \varepsilon^3 \frac{\{F_1, \{F_1, \{F_1, \xi_i'\}'\}'\}'}{3!}$$

$$- \varepsilon^2\{F_2, \xi_i'\}' + \varepsilon^3\{F_1, \{F_2, \xi_i'\}'\}' - \varepsilon^3\{F_3, \xi_i'\}' \qquad (12)$$

where $i = 1, 2, 3, 4$, $\xi_1 = I_1$, $\xi_2 = I_2$, $\xi_3 = \theta_1$, $\xi_4 = \theta_2$, $\xi_1' = I_1'$, $\xi_2' = I_2'$, $\xi_3' = \theta_1'$, $\xi_4' = \theta_2'$.

Here $I(t), \theta(t)$ represent the solutions of the EOM for the Henon–Heiles Hamiltonian, while $I'(t), \theta'(t)$ represent the solutions for the harmonic oscillator Hamiltonian.

4. Numerical results

Using a 4th-order Runge–Kutta–Gill adaptive ODE solver, the EOM for the Henon–Heiles system were solved and the invariants predicted by third order perturbation theory were computed. Figures 1(a) and 1(b) give the relative variation in one of the constants of motion (I_1') for two different energies: 1(a) for the regular regime of the perturbed Hamiltonian and 1(b) for the chaotic regime of the Hamiltonian, for first, second and third order perturbation theory. (In the figures, relative deviation in $I_1'(t)$ is calculated as $2*(I_1'(t) - I_1'(0))/(I_1'(t) + I_1'(0))$.) Figure 2 shows the third order prediction at different energy values. With increase in E the constancy becomes worse i.e., error increases but higher order results remain superior to lower order results for some time, at larger time the error become too large.

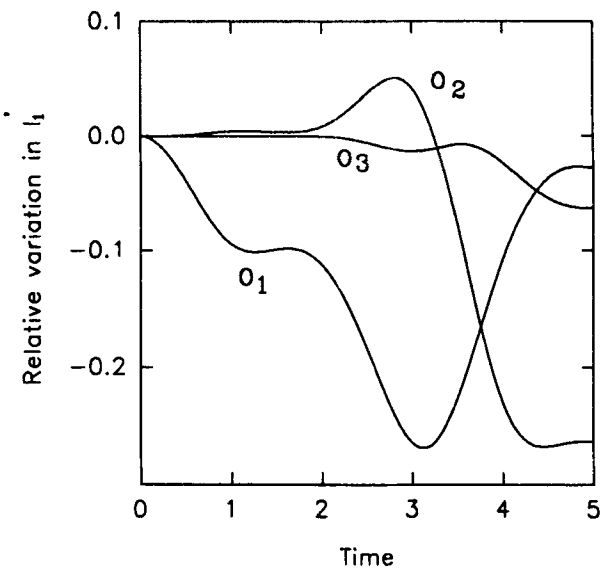

Figure 1a. Relative variation in predicted time-dependent constant of motion I_1' for $E = 0{\cdot}034$, O_1, O_2 and O_3 represent results of first, second and third order perturbation theory results respectively.

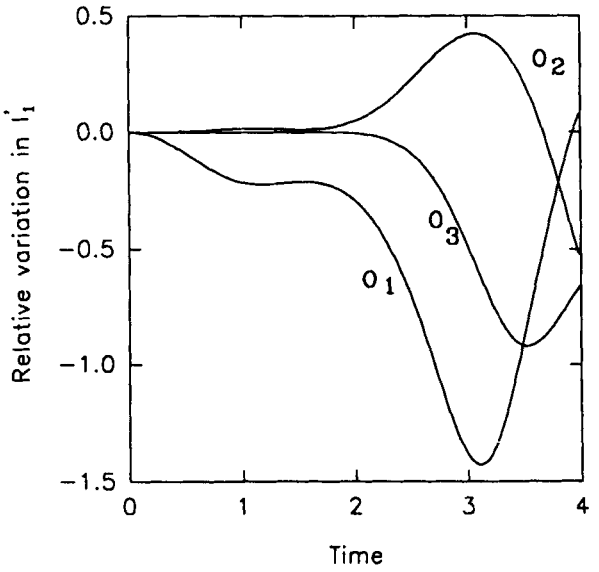

Figure 1b. Same as figure 1a for $E = 0{\cdot}112$.

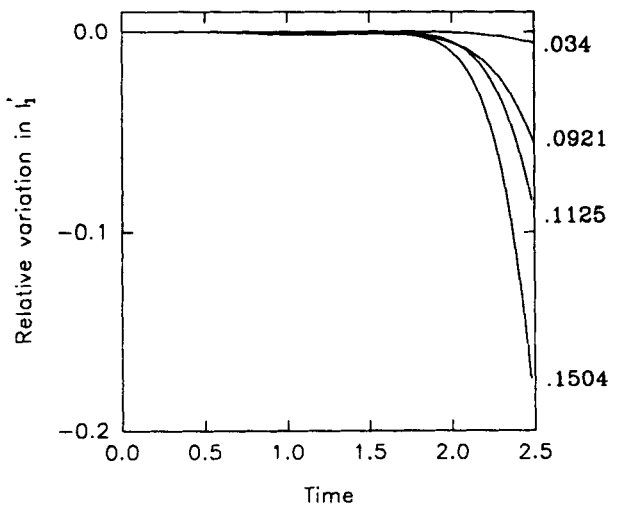

Figure 2. Relative variation in predicted constant of motion at third order, at different E values for the Henon–Heiles system.

For comparing the solutions, the same Runge–Kutta–Gill ODE solver was used and results were compared with the predictions of (12). These results are summarized in figures 3(a) and 3(b) (solid lines), which show the relative error in predicted solutions with respect to numerical solutions; for the first, second and third order perturbation theory. (The relative error in $I_1(t)$ is, $2(I_{1p}(t) - I_{1n}(t))/(I_{1p}(t) - I_{1n}(t))$ where I_{1p} is the predicted solution and I_{1n} is the numerical solution.) Figure 4 shows the results of

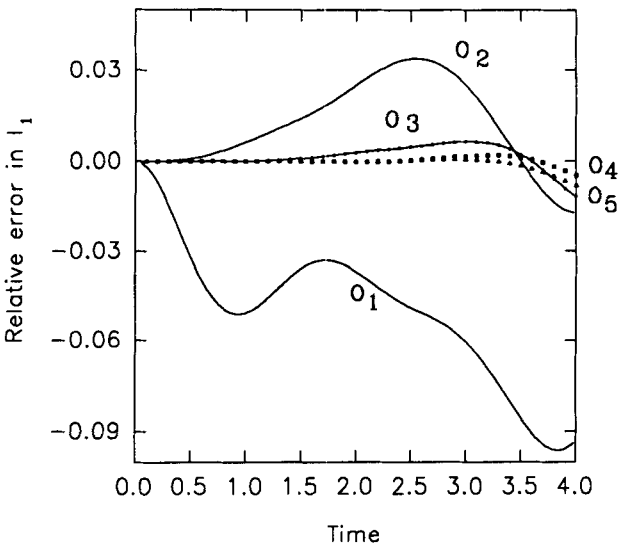

Figure 3a. Relative error in predicted solution for I_1 for the Henon–Heiles system at $E = 0{\cdot}034$. O_1, O_2 and O_3 represent results of first, second and third order perturbation theory results respectively. Dotted curves show numerically calculated higher orders.

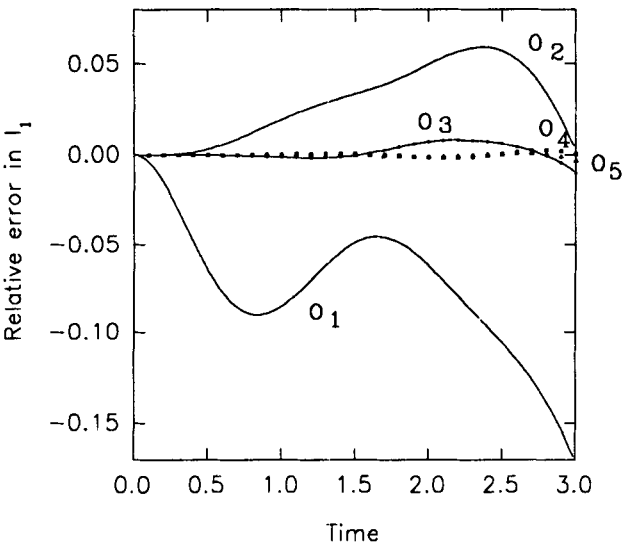

Figure 3b. Same as figure 3a for $E = 0{\cdot}112$.

application of the third order perturbation theory for a spectrum of energies ranging from the regular to the chaotic regime.

We also tested perturbation theory for two orbits of the Henon–Heiles system, one of which is known to be chaotic and the other regular (as seen from their Poincare

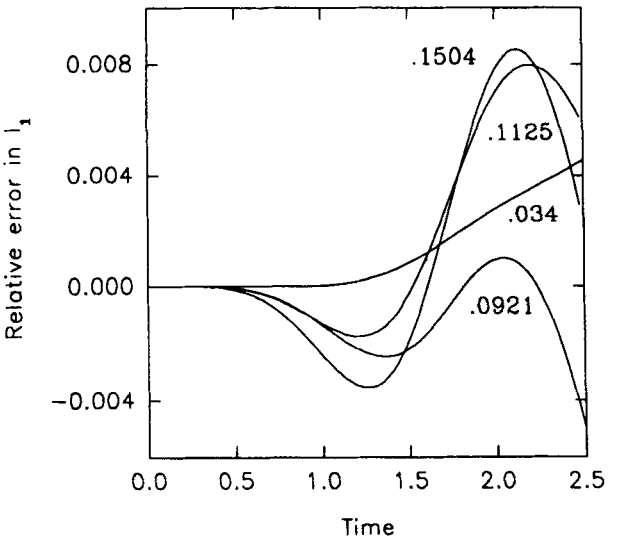

Figure 4. Relative error in third order predicted solution for I_1 for the Henon–Heiles system at different E values.

sections). Figure 5(a) shows the behaviour of the constants of motion for a chaotic trajectory and 5(b) shows the same for a regular trajectory at the same energy value. Figures 6(a) and 6(b) are the Poincare sections for the initial conditions of 5(a) and 5(b) respectively.

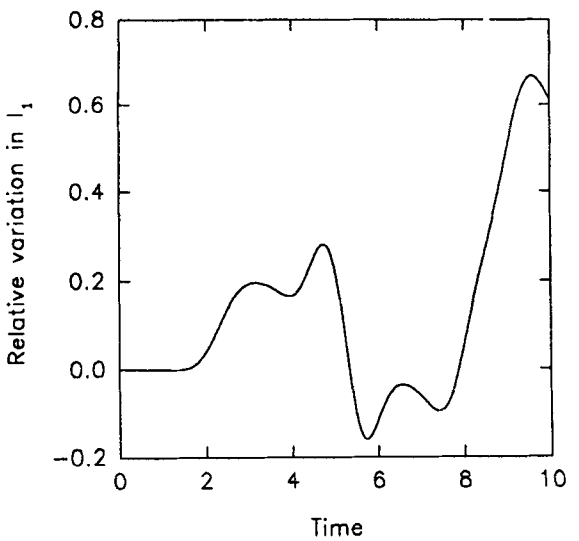

Figure 5a. Relative variation in third order predicted constant of motion I'_1 for the Henon–Heiles system for a chaotic trajectory at $E = 0{\cdot}125$.

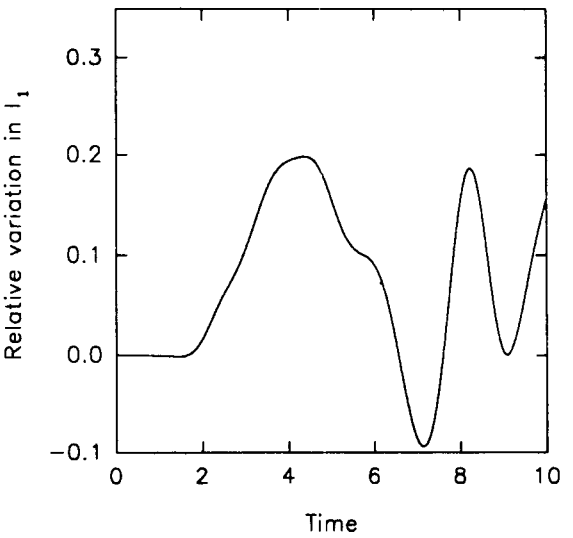

Figure 5b. Relative variation in third order predicted constant of motion I_1' for the Henon–Heiles system for a regular trajectory at $E = 0{\cdot}125$.

5. Convergence of the series

As it is obvious from the numerical results, the prediction of the perturbation theory does not seem to be in agreement with the numerical results. This may be due to two reasons,

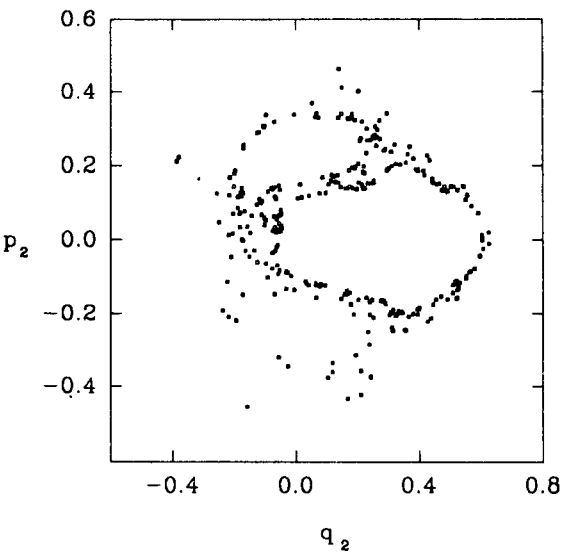

Figure 6a. Poincare section of the chaotic trajectory of figure 5a.

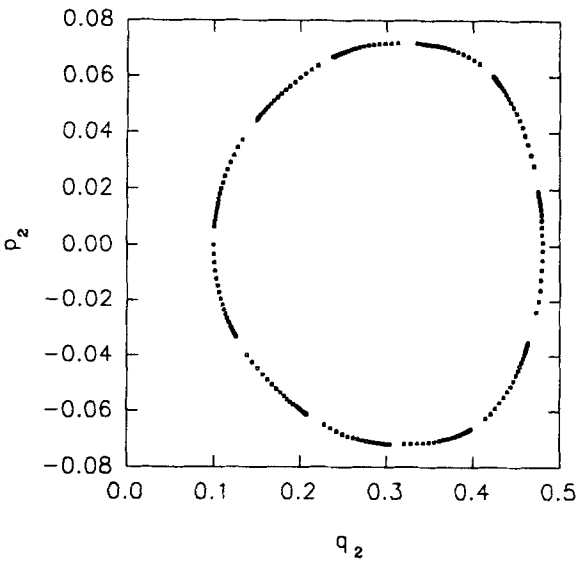

Figure 6b. Poincare section of the regular trajectory of figure 5b.

1. Only first few orders of the perturbation series are considered, in which case the perturbation theory should agree with the numerical results at higher energies, and larger times if enough number of terms in the perturbation series are considered.
2. Contrary to our assumption that the generating function is analytic in the complex ε plane, there exists a singularity; in that case one can expect the perturbation theory to converge only in the region where the distance of ε from origin is less than that of the radius of convergence.

To investigate which one of the former reasons is responsible for the disagreement of the perturbation theory with numerical calculations we analyzed the analytic structure of the system in complex ε real t space [1].

For the initial conditions selected for figure 2, the equations were integrated in real time for 100 different ε values lying on a circle with radius 0·01 and centre $\varepsilon = (0, 0)$. The failure of the integration subroutine was considered as existence of singularity. Three different subroutines drkgs (SSP; Runge-Kutta), d02baf (IMSL) and d02ebf (IMSL stiff equation solver) were used; the routine d02ebf fails with ihalf = 2, which indicates presence of singularity. The results of the calculations are shown in table 1. The smallest time at which one of the points on the circle becomes singular is given.

It is not expected for the above test to work for any general Hamiltonian because it does not detect branch point singularities, but in this specific case it turns out that a branch point in q_1 corresponds to a branch point in p_1 with negative exponent (this can be seen from Painleve analysis [6]) and same is true for q_2 and p_2. Thus even though there are singularities where the position variables remain finite, the corresponding momentum variables become infinite, hence the time at which one of the variables become infinity is the same at which another variable has a branch point with finite value.

Table 1. Complex-ε singularities in real time.

Initial conditions				Time for appearance of singularity		
q_1	q_2	p_1	p_2	drkgs	d02baf	d02ebf
4·47214	4·89898	0	0	$t > 200$		
14·1421	21·4476	0	0	111·6145	$111{\cdot}8 < t < 111{\cdot}9$	$111{\cdot}8 < t < 111{\cdot}9$
30	24·4949	0	0	27·0544	$27{\cdot}3 < t < 27{\cdot}4$	$27{\cdot}3 < t < 27{\cdot}4$
26·6648	31·9374	0	0	19·37	$19{\cdot}6 < t < 19{\cdot}7$	$19{\cdot}6 < t < 19{\cdot}7$
34·9285	34·9285	0	0	13·4095	$13{\cdot}6 < t < 13{\cdot}7$	$13{\cdot}6 < t < 13{\cdot}7$

This analysis indicate that the perturbation theory should be convergent for given initial conditions and ε for larger time values than what is seen in figure 2, thus the reason for disagreement should be truncation of the series rather than existence of a singularity. To verify this reasoning we did a numerical study as follows.

When one uses the generating functions for mapping of the solution for unperturbed Hamiltonian into the solution of the perturbed Hamiltonian, the result is the solution ξ of H in terms of solutions ξ' of H_0, t and a power series in ε. In this series for ξ the coefficient of a term ε^n is $(1/n!)(\mathrm{d}^n\xi/\mathrm{d}\varepsilon^n)$. We did numerical calculations for $\mathrm{d}^n\xi/\mathrm{d}\varepsilon^n$ using

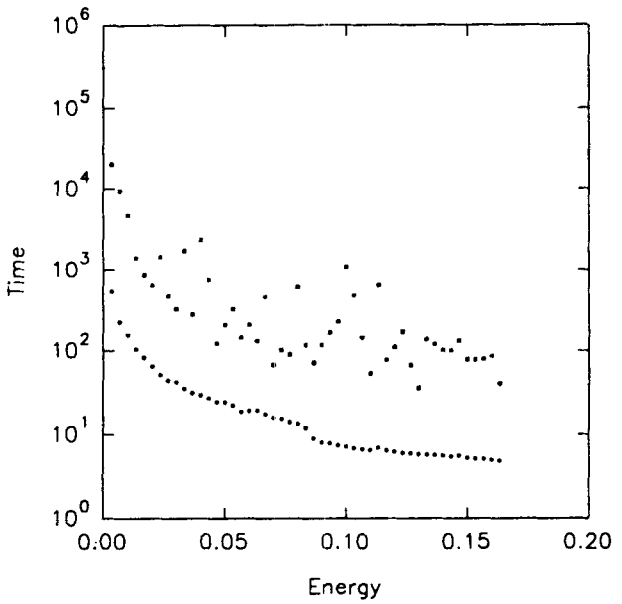

Figure 7. At fixed energy 100 different initial conditions are chosen randomly and each initial conditions is evolved in time with all the 100 different ε values equally spaced on a circle of radius 1 and centre (0, 0) in the complex-ε plane. The minimum time at which one of the points in complex-ε circle encounters a singularity is noted. From the minimum time thus found for each initial conditions at a fixed energy the minimum and maximum times are plotted against energy.

contour integral definition for derivatives and matched our numerical results with the analytical results predicted by perturbation theory. As can be seen from figure 3, where the dotted curves denote numerically calculated higher orders, the third order analytical predictions are well in agreement with numerical values and the fourth and fifth order numerical results show that a higher order analytical calculation would make the predictions better.

To explain the worsening of perturbation theory at higher energies, we did the following calculation. We selected 100 different initial conditions randomly for each of 49 different energies and for each set of initial conditions we fixed 100 points on the complex ε circle with radius 1 and centre (0, 0) and calculated the minimum value of time at which one of the points on the circle became singular. This value of time is the minimum real time at which there is a singularity in the complex ε plane and this singularity will decide the radius of convergence for the perturbation theory. Figure 7 shows the minimum and maximum values of the above minimum time from the 100 initial conditions at each energy value versus the energy. The minimum time value in the figure is the value up to which the perturbation theory will converge if enough number of orders are calculated, whereas the maximum at each energy shows that there are some initial conditions for which the perturbation theory will converge for very large time without any need for analytical continuation of the generator.

It thus appears from our analysis that the time-dependent canonical perturbation theory can be used for studying the Henon–Heiles system, the fact that the results show disagreement with numerical results is to be attributed to the low order of perturbation theory used.

Appendix A. Generating functions

We give below the form of the generating functions up to order ε^3.

$$
\begin{aligned}
F_1 = {} & \frac{-(I_2^{3/2}\sin(3t-3\theta_2))}{9\sqrt{2}} + \sqrt{2}I_1\sqrt{I_2}\sin(t-\theta_2) \\
& - \frac{I_2^{3/2}\sin(t-\theta_2)}{\sqrt{2}} + \frac{I_2\sqrt{I_2}\sin(3t-2\theta_1-\theta_2)}{3\sqrt{2}} \\
& + \frac{I_1\sqrt{I_2}\sin(2\theta_1-\theta_2)}{\sqrt{2}} + \sqrt{2}I_1\sqrt{I_2}\sin(\theta_2) \\
& - \frac{I_2^{3/2}\sin(\theta_2)}{\sqrt{2}} - \frac{I_2^{3/2}\sin(3\theta_2)}{9\sqrt{2}} \\
& + \frac{I_1\sqrt{I_2}\sin(t-2\theta_1+\theta_2)}{\sqrt{2}} + \frac{I_1\sqrt{I_2}\sin(2\theta_1+\theta_2)}{3\sqrt{2}} \\
F_2 = {} & \frac{-5I_1^2 t}{12} + \frac{I_1 I_2 t}{3} - \frac{5I_2^2 t}{12} - \frac{7I_1 I_2 t\cos(2\theta_1-2\theta_2)}{6} \\
& + \frac{3I_1^2\sin(t)}{8} - \frac{I_1 I_2\sin(t)}{2} + \frac{3I_2^2\sin(t)}{8} + \frac{I_1^2\sin(3t)}{72}
\end{aligned}
$$

$$+\frac{I_1 I_2 \sin(3t)}{18}+\frac{I_2^2 \sin(3t)}{72}+\frac{I_1^2 \sin(t-4\theta_1)}{24}$$

$$-\frac{I_1^2 \sin(3t-4\theta_1)}{24}+\frac{I_1^2 \sin(4t-4\theta_1)}{48}-\frac{I_1^2 \sin(2t-2\theta_1)}{6}$$

$$-\frac{I_1 I_2 \sin(2t-2\theta_1)}{6}+\frac{I_1^2 \sin(3t-2\theta_1)}{12}+\frac{I_1 I_2 \sin(3t-2\theta_1)}{12}$$

$$-\frac{I_1^2 \sin(2\theta_1)}{6}-\frac{I_1 I_2 \sin(2\theta_1)}{6}+\frac{I_1^2 \sin(4\theta_1)}{48}$$

$$+\frac{I_1^2 \sin(t+2\theta_1)}{12}+\frac{I_1 I_2 \sin(t+2\theta_1)}{12}+\frac{I_2^2 \sin(t-4\theta_2)}{24}$$

$$-\frac{I_2^2 \sin(3t-4\theta_2)}{24}+\frac{I_2^2 \sin(4t-4\theta_2)}{48}-\frac{I_1 I_2 \sin(2t-2\theta_2)}{6}$$

$$-\frac{I_2^2 \sin(2t-2\theta_2)}{6}+\frac{I_1 I_2 \sin(3t-2\theta_2)}{12}+\frac{I_2^2 \sin(3t-2\theta_2)}{12}$$

$$+\frac{I_1 I_2 \sin(t-2\theta_1-2\theta_2)}{12}-\frac{I_1 I_2 \sin(3t-2\theta_1-2\theta_2)}{12}$$

$$+\frac{I_1 I_2 \sin(4t-2\theta_1-2\theta_2)}{24}+\frac{5I_1 I_2 \sin(t+2\theta_1-2\theta_2)}{8}$$

$$-\frac{I_1 I_2 \sin(3t+2\theta_1-2\theta_2)}{72}-\frac{I_1 I_2 \sin(2\theta_2)}{6}-\frac{I_2^2 \sin(2\theta_2)}{6}$$

$$+\frac{I_2^2 \sin(4\theta_2)}{48}+\frac{I_1 I_2 \sin(t+2\theta_2)}{12}+\frac{I_2^2 \sin(t+2\theta_2)}{12}$$

$$+\frac{5I_1 I_2 \sin(t-2\theta_1+2\theta_2)}{8}-\frac{I_1 I_2 \sin(3t-2\theta_1+2\theta_2)}{72}$$

$$+\frac{I_1 I_2 \sin(2\theta_1+2\theta_2)}{24}$$

$$F_3=\frac{-7I_1 I_2^{3/2} t\cos(2\theta_1-3\theta_2)}{2\sqrt{2}}-\frac{13I_1^2\sqrt{I_2}\, t\cos(2\theta_1-\theta_2)}{3\sqrt{2}}$$

$$+\frac{37I_1 I_2^{3/2} t\cos(2\theta_1-\theta_2)}{6\sqrt{2}}-\frac{7I_1^2\sqrt{I_2}\, t\cos(4\theta_1-\theta_2)}{18\sqrt{2}}$$

$$+\frac{11I_1^2\sqrt{I_2}\, t\cos(\theta_2)}{6\sqrt{2}}-\frac{13I_1 I_2^{3/2} t\cos(\theta_2)}{3\sqrt{2}}$$

$$+\frac{5I_2^{5/2} t\cos(\theta_2)}{6\sqrt{2}}-\frac{4\sqrt{2}I_1 I_2^{3/2} t\cos(3\theta_2)}{9}$$

$$+\frac{5I_2^{5/2}t\cos(3\theta_2)}{18\sqrt{2}}-\frac{2\sqrt{2}I_1^2\sqrt{I_2}t\cos(2\theta_1+\theta_2)}{9}$$

$$+\frac{I_1I_2^{3/2}t\cos(2\theta_1+\theta_2)}{3\sqrt{2}}+\frac{I_2^{5/2}\sin(t-5\theta_2)}{18\sqrt{2}}$$

$$-\frac{I_2^{5/2}\sin(2t-5\theta_2)}{216\sqrt{2}}-\frac{7I_2^{5/2}\sin(3t-5\theta_2)}{108\sqrt{2}}$$

$$+\frac{5I_2^{5/2}\sin(4t-5\theta_2)}{72\sqrt{2}}-\frac{2\sqrt{2}I_2^{5/2}\sin(5t-5\theta_2)}{135}$$

$$+\frac{I_2^{5/2}\sin(6t-5\theta_2)}{216\sqrt{2}}+\frac{5I_1I_2^{3/2}\sin(t-3\theta_2)}{9\sqrt{2}}$$

$$-\frac{7I_2^{5/2}\sin(t-3\theta_2)}{36\sqrt{2}}-\frac{I_1I_2^{3/2}\sin(2t-3\theta_2)}{18\sqrt{2}}$$

$$-\frac{13I_2^{5/2}\sin(2t-3\theta_2)}{72\sqrt{2}}+\frac{\sqrt{2}I_1I_2^{3/2}\sin(3t-3\theta_2)}{27}$$

$$+\frac{5I_2^{5/2}\sin(3t-3\theta_2)}{27\sqrt{2}}-\frac{I_1I_2^{3/2}\sin(4t-3\theta_2)}{18\sqrt{2}}$$

$$-\frac{I_2^{5/2}\sin(4t-3\theta_2)}{18\sqrt{2}}+\frac{I_1I_2^{3/2}\sin(6t-3\theta_2)}{162\sqrt{2}}$$

$$+\frac{I_2^{5/2}\sin(6t-3\theta_2)}{648\sqrt{2}}-\frac{I_1I_2^{3/2}\sin(t-2\theta_1-3\theta_2)}{9\sqrt{2}}$$

$$+\frac{I_1I_2^{3/2}\sin(2t-2\theta_1-3\theta_2)}{108\sqrt{2}}+\frac{7I_1I_2^{3/2}\sin(3t-2\theta_1-3\theta_2)}{54\sqrt{2}}$$

$$-\frac{5I_1I_2^{3/2}\sin(4t-2\theta_1-3\theta_2)}{36\sqrt{2}}+\frac{4\sqrt{2}I_1I_2^{3/2}\sin(5t-2\theta_1-3\theta_2)}{135}$$

$$-\frac{I_1I_2^{3/2}\sin(6t-2\theta_1-3\theta_2)}{108\sqrt{2}}-\frac{355I_1I_2^{3/2}\sin(2\theta_1-3\theta_2)}{216\sqrt{2}}$$

$$+\frac{49\sqrt{2}I_1I_2^{3/2}\sin(t+2\theta_1-3\theta_2)}{27}-\frac{13I_1I_2^{3/2}\sin(2t+2\theta_1-3\theta_2)}{18\sqrt{2}}$$

$$-\frac{I_1I_2^{3/2}\sin(3t+2\theta_1-3\theta_2)}{54\sqrt{2}}+\frac{7I_1I_2^{3/2}\sin(4t+2\theta_1-3\theta_2)}{216\sqrt{2}}$$

$$-\frac{\sqrt{2}I_1^2\sqrt{I_2}\sin(t-\theta_2)}{3}+\frac{23\sqrt{2}I_1I_2^{3/2}\sin(t-\theta_2)}{9}$$

$$-\frac{20\sqrt{2}I_2^{5/2}\sin(t-\theta_2)}{27}-\frac{I_1^2\sqrt{I_2}\sin(2t-\theta_2)}{2\sqrt{2}}$$

$$-\frac{2\sqrt{2}I_1I_2^{3/2}\sin(2t-\theta_2)}{3}+\frac{11I_2^{5/2}\sin(2t-\theta_2)}{18\sqrt{2}}$$

$$+\frac{5I_1^2\sqrt{I_2}\sin(3t-\theta_2)}{18\sqrt{2}}+\frac{I_1I_2^{3/2}\sin(3t-\theta_2)}{9\sqrt{2}}$$

$$-\frac{7I_2^{5/2}\sin(3t-\theta_2)}{54\sqrt{2}}-\frac{I_1^2\sqrt{I_2}\sin(4t-\theta_2)}{24\sqrt{2}}$$

$$+\frac{I_1I_2^{3/2}\sin(4t-\theta_2)}{36\sqrt{2}}+\frac{I_2^{5/2}\sin(4t-\theta_2)}{216\sqrt{2}}$$

$$-\frac{I_1^2\sqrt{I_2}\sin(t-4\theta_1-\theta_2)}{6\sqrt{2}}+\frac{I_1^2\sqrt{I_2}\sin(2t-4\theta_1-\theta_2)}{72\sqrt{2}}$$

$$+\frac{7I_1^2\sqrt{I_2}\sin(3t-4\theta_1-\theta_2)}{36\sqrt{2}}-\frac{5I_1^2\sqrt{I_2}\sin(4t-4\theta_1-\theta_2)}{24\sqrt{2}}$$

$$+\frac{2\sqrt{2}I_1^2\sqrt{I_2}\sin(5t-4\theta_1-\theta_2)}{45}-\frac{I_1^2\sqrt{I_2}\sin(6t-4\theta_1-\theta_2)}{72\sqrt{2}}$$

$$+\frac{I_1^2\sqrt{I_2}\sin(t-2\theta_1-\theta_2)}{3\sqrt{2}}-\frac{I_1I_2^{3/2}\sin(t-2\theta_1-\theta_2)}{6\sqrt{2}}$$

$$+\frac{I_1^2\sqrt{I_2}\sin(2t-2\theta_1-\theta_2)}{2\sqrt{2}}+\frac{5I_1I_2^{3/2}\sin(2t-2\theta_1-\theta_2)}{12\sqrt{2}}$$

$$-\frac{7\sqrt{2}I_1^2\sqrt{I_2}\sin(3t-2\theta_1-\theta_2)}{27}-\frac{2\sqrt{2}I_1I_2^{3/2}\sin(3t-2\theta_1-\theta_2)}{9}$$

$$+\frac{I_1^2\sqrt{I_2}\sin(4t-2\theta_1-\theta_2)}{6\sqrt{2}}+\frac{I_1I_2^{3/2}\sin(4t-2\theta_1-\theta_2)}{6\sqrt{2}}$$

$$-\frac{I_1^2\sqrt{I_2}\sin(6t-2\theta_1-\theta_2)}{162\sqrt{2}}-\frac{I_1I_2^{3/2}\sin(6t-2\theta_1-\theta_2)}{108\sqrt{2}}$$

$$+\frac{85I_1^2\sqrt{I_2}\sin(2\theta_1-\theta_2)}{36\sqrt{2}}-\frac{185I_1I_2^{3/2}\sin(2\theta_1-\theta_2)}{72\sqrt{2}}$$

$$+\frac{5I_1^2\sqrt{I_2}\sin(t+2\theta_1+\theta_2)}{3\sqrt{2}}-\frac{13I_1I_2^{3/2}\sin(t+2\theta_1-\theta_2)}{6\sqrt{2}}$$

$$-\frac{I_1^2\sqrt{I_2}\sin(2t+2\theta_1-\theta_2)}{9\sqrt{2}}-\frac{\sqrt{2}I_1I_2^{3/2}\sin(2t+2\theta_1-\theta_2)}{9}$$

$$+\frac{I_1 I_2^{3/2}\sin(3t+2\theta_1-\theta_2)}{9\sqrt{2}}+\frac{5I_1^2\sqrt{I_2}\sin(4\theta_1-\theta_2)}{54\sqrt{2}}$$

$$+\frac{I_1^2\sqrt{I_2}\sin(t+4\theta_1-\theta_2)}{6\sqrt{2}}-\frac{I_1^2\sqrt{I_2}\sin(3t+4\theta_1-\theta_2)}{324\sqrt{2}}$$

$$-\frac{5I_1^2\sqrt{I_2}\sin(\theta_2)}{24\sqrt{2}}+\frac{85I_1 I_2^{3/2}\sin(\theta_2)}{36\sqrt{2}}$$

$$-\frac{155I_2^{5/2}\sin(\theta_2)}{216\sqrt{2}}+\frac{5I_1 I_2^{3/2}\sin(3\theta_2)}{54\sqrt{2}}$$

$$-\frac{5I_2^{5/2}\sin(3\theta_2)}{27\sqrt{2}}+\frac{43I_2^{5/2}\sin(5\theta_2)}{1080\sqrt{2}}$$

$$-\frac{I_1^2\sqrt{I_2}\sin(t+\theta_2)}{2\sqrt{2}}+\frac{5I_1 I_2^{3/2}\sin(t+\theta_2)}{3\sqrt{2}}$$

$$-\frac{7I_2^{5/2}\sin(t+\theta_2)}{18\sqrt{2}}-\frac{I_1^2\sqrt{I_2}\sin(2t+\theta_2)}{3\sqrt{2}}$$

$$-\frac{I_1 I_2^{3/2}\sin(2t+\theta_2)}{9\sqrt{2}}+\frac{2\sqrt{2}I_2^{5/2}\sin(2t+\theta_2)}{27}$$

$$+\frac{I_1^2\sqrt{I_2}\sin(3t+\theta_2)}{9\sqrt{2}}-\frac{I_2^{5/2}\sin(3t+\theta_2)}{27\sqrt{2}}$$

$$+\frac{I_1^2\sqrt{I_2}\sin(t-4\theta_1+\theta_2)}{4\sqrt{2}}+\frac{I_1^2\sqrt{I_2}\sin(2t-4\theta_1+\theta_2)}{24\sqrt{2}}$$

$$-\frac{I_1^2\sqrt{I_2}\sin(3t-4\theta_1+\theta_2)}{27\sqrt{2}}+\frac{I_1^2\sqrt{I_2}\sin(6t-4\theta_1+\theta_2)}{648\sqrt{2}}$$

$$+\frac{23\sqrt{2}I_1^2\sqrt{I_2}\sin(t-2\theta_1+\theta_2)}{9}-\frac{26\sqrt{2}I_1 I_2^{3/2}\sin(t-2\theta_1+\theta_2)}{9}$$

$$-\frac{2\sqrt{2}I_1^2\sqrt{I_2}\sin(2t-2\theta_1+\theta_2)}{3}+\frac{5I_1 I_2^{3/2}\sin(2t-2\theta_1+\theta_2)}{6\sqrt{2}}$$

$$+\frac{I_1^2\sqrt{I_2}\sin(3t-2\theta_1+\theta_2)}{9\sqrt{2}}+\frac{I_1 I_2^{3/2}\sin(3t-2\theta_1+\theta_2)}{6\sqrt{2}}$$

$$+\frac{I_1^2\sqrt{I_2}\sin(4t-2\theta_1+\theta_2)}{36\sqrt{2}}-\frac{5I_1 I_2^{3/2}\sin(4t-2\theta_1+\theta_2)}{72\sqrt{2}}$$

$$+\frac{25I_1^2\sqrt{I_2}\sin(2\theta_1+\theta_2)}{54\sqrt{2}}+\frac{5I_1 I_2^{3/2}\sin(2\theta_1+\theta_2)}{18\sqrt{2}}$$

$$-\frac{I_1 I_2^{3/2}\sin(t+2\theta_1+\theta_2)}{3\sqrt{2}}+\frac{I_1^2\sqrt{I_2}\sin(3t+2\theta_1+\theta_2)}{81\sqrt{2}}$$
$$+\frac{I_1 I_2^{3/2}\sin(3t+2\theta_1+\theta_2)}{54\sqrt{2}}-\frac{43I_1^2\sqrt{I_2}\sin(4\theta_1+\theta_2)}{360\sqrt{2}}$$
$$+\frac{I_1^2\sqrt{I_2}\sin(t+4\theta_1+\theta_2)}{36\sqrt{2}}+\frac{2\sqrt{2}I_1 I_2^{3/2}\sin(t+3\theta_2)}{9}$$
$$-\frac{I_2^{5/2}\sin(t+3\theta_2)}{18\sqrt{2}}-\frac{I_1 I_2^{3/2}\sin(3t+3\theta_2)}{81\sqrt{2}}$$
$$-\frac{I_2^{5/2}\sin(3t+3\theta_2)}{324\sqrt{2}}+\frac{23I_1 I_2^{3/2}\sin(t-2\theta_1+3\theta_2)}{18\sqrt{2}}$$
$$+\frac{I_2 I_2^{3/2}\sin(2t-2\theta_1+3\theta_2)}{27\sqrt{2}}-\frac{I_1 I_2^{3/2}\sin(3t-2\theta_1+3\theta_2)}{27\sqrt{2}}$$
$$-\frac{43I_1 I_2^{3/2}\sin(2\theta_1+3\theta_2)}{540\sqrt{2}}+\frac{I_1 I_2^{3/2}\sin(t+2\theta_1+3\theta_2)}{54\sqrt{2}}$$
$$-\frac{I_2^{5/2}\sin(t+5\theta_2)}{108\sqrt{2}}.$$

References

[1] B R Sitaram and Mitaxi P Mehta, *Pramana – J. Phys.* **45**, 141 (1995)
[2] M Henon and C Heiles, *Astron. J.* **69**, 73 (1964)
[3] M V Berry, in Topics in nonlinear dynamiçs: A tribute to Sir Edward Bullard, *AIP conference proceedings*, edited by S Jorna (American Institute of Physics, New York, 1978) p. 37
[4] M Tabor, *Chaos and integrability in nonlinear dynamics: An introduction* (John Wiley and Sons, New York, 1989) p. 106
[5] F A Gustavson, *Astron. J.* **71**, 670 (1966)
[6] Y F Chang, M Tabor and J Weiss, *J. Math. Phys.* **23**, 531 (1982)